Available online at www.sciencedirect.com
ScienceDirect
International Journal of Solids and Structures 45 (2008) 2723–2736
INTERNATIONAL JOURNAL OF SOLIDS AND STRUCTURES
www.elsevier.com/locate/ijsolstr

Normal and tangential compliances of interface of rough surfaces with contacts of elliptic shape

Igor Sevostianov [a,*], Mark Kachanov [b]

[a] Department of Mechanical Engineering, New Mexico State University, PO Box 30001, Las Cruces, NM 88003, USA
[b] Department of Mechanical Engineering, Tufts University, Medford, MA 02155, USA

Received 26 October 2007; received in revised form 26 December 2007
Available online 18 January 2008

Abstract

The incremental compliances, normal and tangential, of an interface between rough surfaces are considered. Contacts are assumed to be elliptic – the shape of Hertzian contacts between any two locally smooth asperities. The ellipses may have diverse eccentricities and random or non-random orientation distribution; in the latter case, the tangential compliance is anisotropic. It is found that the Hertzian contacts and "welded" zones of the same geometry produce the same incremental compliances. Microstructural characteristics ξ of the interface that controls its incremental compliances is identified. For the circular contacts, ξ is the sum $\sum\sqrt{A_k}$ where A_k is kth contact area; in the more general case of elliptic contacts, each A_k enters in product with its shape factor dependent on the ellipse aspect ratio. The mentioned in-plane tangential anisotropy is relatively mild, even for parallel strongly elongated elliptic contacts. This is due to weakness of the anisotropy for a single elliptic contact (or external elliptic crack). Comparison of the latter to the *internal* crack of the same elliptic geometry shows that whereas the anisotropy is mild for both crack types, it is weaker for the external crack, in which case it is also less sensitive to Poisson's ratio.

Keywords: Rough surface; Compliance; Contact

1. Introduction

We discuss an interface between two plates formed by multiple isolated contacts. The compliance of such an interface has been analyzed in a number of works, both theoretical and experimental, that emphasized different aspects of the problem. It appears that the main focus has been on non-linearities of the stress–displacement curve under increasing compression. Relating this curve to relevant features of microgeometry is a difficult problem (particularly in the shear mode), and we refer to Baltazar et al. (2002) for an overview of related literature and to Walsh and Zhu (2004) and Sevostianov and Kacha-

* Corresponding author. Tel.: +1 505 6463322; fax: +1 505 6466111.
E-mail addresses: igor@saratoga.nmsu.edu (I. Sevostianov), mark.kachanov@tufts.edu (M. Kachanov).

0020-7683/$ - see front matter © 2008 Elsevier Ltd. All rights reserved.
doi:10.1016/j.ijsolstr.2007.12.024

nov (2008) for recent contributions. We also mention that elliptic contacts between two nominally flat surfaces were discussed in the context of fluid permeability of fractured rocks by Zimmerman et al. (1992).

The present work focuses on the *incremental* compliances of the interface (normal and tangential) and on the microstructural parameters that control them. The incremental compliances are relevant, in particular, for various wave propagation problems where the stress levels are, typically, too low to cause non-linearities. If the wavelength is much larger than sizes of microstructural features, these data reflect, among other factors, the effective incremental compliances of the interface. Applications range from large scale fractures encountered in rock mechanics (where information on fractures has to be extracted from wavespeeds, with the account of contacts between crack faces), to ultrasonic examination of imperfect interfaces.

One of the relevant problems is comparative analysis of the effects produced by contacts of the Hertzian type, with cusp-like geometry along the edge (called sometimes "kissing" bonds in the ultrasonics literature) and "welded" areas. Refraining from a comprehensive review, we mention the work of Nagy (1992) where these issues are discussed in the context of ultrasonics. Comparative analysis of the Hertzian vs "welded" contact geometries is one of the focal points of the present work.

Some of the problems discussed here have been examined in the work of Sevostianov and Kachanov (2008) where non-linearities under increasing compression were also discussed. The work assumed circular contact zones; for such geometries, the incremental compliances (the normal and the tangential ones) are controlled by the sum of the square roots of contacting areas $\sum\sqrt{A_k}$ – independently of whether the contacts are Hertzian or represent "welded" areas. The assumption of circular shapes may, however, be too restrictive for applications. The present work considers the elliptic contact zones that correspond to the general case of Hertzian contacts of locally smooth asperities. In this case, the shape factors – the distribution of ellipses' eccentricities and orientations – play an important role, and the controlling microstructural parameter $\sum\sqrt{A_k}$ has to be modified to reflect them.

We first consider an individual contact, and examine two contact types – the Hertzian ones and "welded" areas. These two cases may be viewed as extreme cases of contact edge microgeometries. Then, we consider multiple elliptic contacts of diverse eccentricities, and examine two cases – random orientations of the eccentricities and non-random, preferential orientations of the contact zones resulting in anisotropic tangential compliance. The latter case corresponds, in particular, to technological processes that have some directionality, such as polishing procedures involving non-circular, preferential polishing directions; another example is given by rock faults that have undergone sliding displacement.

2. Elliptic contact zone: Hertzian contact vs "welded area

According to the Hertz theory (see, for example, Johnson, 1985), the contact between any two locally smooth asperities pressed against one another has the elliptic shape. We denote by a, b the major and the minor axes of the ellipse, by $\gamma = b/a \leqslant 1$ its aspect ratio and by $A = \pi ab$ its area; E_0, ν_0 denote Young's modulus and Poisson's ratio of the material. We examine the incremental compliances of the contact, normal and tangential, and compare them to the ones of the "welded" area of the same elliptic shape.

2.1. Normal and tangential compliances of the elliptic Hertzian contact

The normal incremental compliance of the Hertzian contact is defined as

$$z_n = \frac{\mathrm{d}w}{\mathrm{d}P} \tag{2.1}$$

where w is the relative displacement of the far points in the normal to the contact plane direction and P is the force transmitted through the contact. Utilizing Mindlin's (1949) results, it can be written in the form:

$$z_n = \frac{2(1-\nu_0^2)}{\pi E_0}\frac{1}{a}\int_0^{\pi/2}\frac{\mathrm{d}\phi}{\sqrt{\sin^2\phi+\gamma^2\cos^2\phi}} = \frac{2(1-\nu_0^2)}{\pi E_0}\frac{1}{a}\int_0^{\pi/2}\frac{\mathrm{d}\phi}{\sqrt{1-(1-\gamma^2)\sin^2\phi}}$$
$$= \frac{\sqrt{\pi}(1-\nu_0^2)}{E_0}\frac{1}{\sqrt{A}}\underbrace{\frac{2\sqrt{\gamma}}{\pi}\mathcal{K}}_{\text{Shape factor } S_n} \tag{2.2}$$

where $\mathcal{K}$ is the complete elliptic integral of the first kind, of argument $\sqrt{1-\gamma^2}$. The compliance is reduced, as compared to a circle of the same area, by the shape factor S_n that is plotted in Fig. 1. It decreases from 1 for a circle to zero in the limit $\gamma \to 0$, indicating that contacts of long narrow shapes are very stiff. Importantly, at $\gamma > 0.4$, the shape factor differs from 1 by less than 5%, indicating that such contact shapes can be replaced by circles of the same area with good accuracy, as far as the incremental normal compliance is concerned.

We now consider the *tangential* incremental compliance of the contact assuming that the elliptic contact area A has been established (for example, by normal loading). It relates the relative shear displacement $\boldsymbol{u}$ of far points to the shear force $\boldsymbol{F}$ transmitted through the contact. The tangential compliance is anisotropic: it depends on the in-plane direction. Therefore, the direction of vector $\boldsymbol{u}$ does not, generally, coincide with the direction of force $\boldsymbol{F}$.

We assume that no frictional slips occur and utilize Mindlin's (1949) results for the tangential compliance in the directions of semiaxes a and b:

$$\begin{Bmatrix} z^{(a)} \\ z^{(b)} \end{Bmatrix} = \frac{\sqrt{\pi}(2-\nu_0)(1+\nu_0)}{2E_0}\frac{1}{\sqrt{A}}\underbrace{\frac{2\sqrt{\gamma}}{\pi}\left[\left(1 \pm \frac{\nu_0}{2-\nu_0}\frac{1+\gamma^2}{1-\gamma^2}\right)\mathcal{K} \mp \frac{2\nu_0}{2-\nu_0}\frac{1}{1-\gamma^2}\mathcal{E}\right]}_{\text{Shape factor } S_\tau} \tag{2.3}$$

where the shape factor for shear, S_τ, dependent on aspect ratio γ is identified, and $\mathcal{E}$ is the complete elliptic integral of the second kind, of argument $\sqrt{1-\gamma^2}$. At $\gamma = 1$ (circular contact), $z^{(a)} = z^{(b)} = \sqrt{\pi}(2-\nu_0)(1+\nu_0)/(2E_0\sqrt{A})$. Figs. 2 and 3 show S_τ as a function of γ and its ratio to the shape factor S_n for the normal compliance.

At Poisson's ratio $\nu_0 = 0$, the orientation dependence of the tangential compliance vanishes, $z^{(a)} = z^{(b)} = 2\sqrt{\gamma}\mathcal{K}/(\sqrt{\pi}E_0\sqrt{A})$. This dependence becomes stronger with increasing ν_0 and with smaller aspect ratio $\gamma = b/a$, but *the anisotropy of the tangential compliance is generally moderate*: at $\nu_0 = 0.25$, the ratio of the maximal incremental compliance (in the direction of the larger semiaxis a) to the minimal one (in the direction of b) is about 1.07 at $\gamma = 0.3$ and 1.13 at $\gamma = 0.1$; at $\nu_0 = 0.5$, these ratios are about 1.25 and 1.37. In the limit $\gamma \to 0$, the ratio $z^{(a)}/z^{(b)} \to 1/(1-\nu_0)$.

We now incorporate both the tangential compliance (2.3) and the normal compliance (2.2) into the *compliance tensor of the elliptic Hertzian contact*:

$$\boldsymbol{z} = z^{(a)}\boldsymbol{e}_a\boldsymbol{e}_a + z^{(b)}\boldsymbol{e}_b\boldsymbol{e}_b + z_n\boldsymbol{n}\boldsymbol{n} \tag{2.4}$$

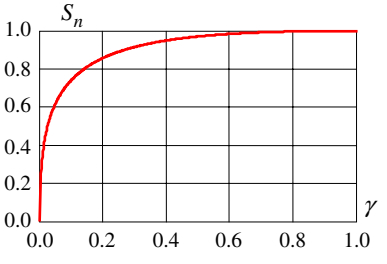

Fig. 1. Shape factor S_n entering Eq. (2.2) for the normal compliance of elliptic contact, as a function of aspect ratio b/a. At aspect ratios $b/a > 0.4$, ellipses can be replaced by circles of the same area with accuracy better than 5%.

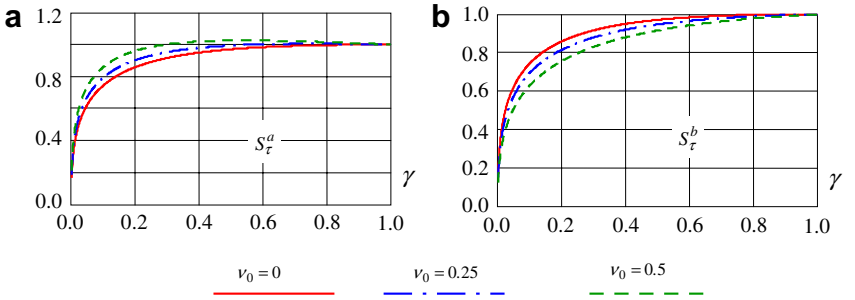

Fig. 2. Shape factors entering Eq. (2.3) for the shear compliances of elliptic contact in the directions of the major, a, and minor, b, ellipse's semiaxes. The difference between the two, that characterizes anisotropy with respect to in-plane directions, is mild, and it vanishes at $\nu_0 = 0$.

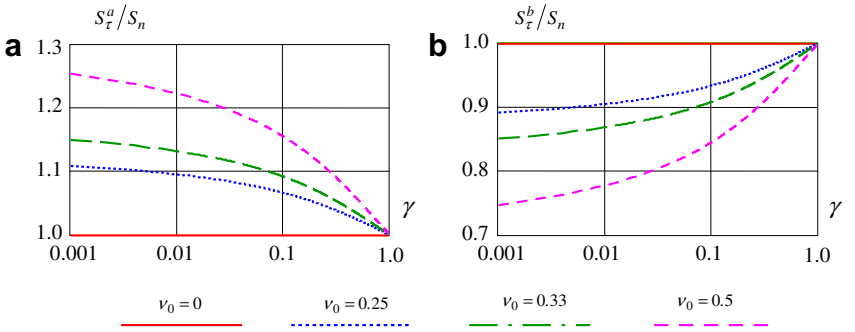

Fig. 3. Ratios of the shear compliances of elliptic contact, in the directions of a and b, to its normal compliance, as functions of the aspect ratio.

($\boldsymbol{e}_a$, $\boldsymbol{e}_b$ are unit vectors along the semiaxes) that gives vector $\boldsymbol{u}$ of relative displacement of far points produced by force $\boldsymbol{F}$ of arbitrary direction transmitted through the contact:

$$\boldsymbol{u} = \boldsymbol{z} \cdot \boldsymbol{F} \tag{2.5}$$

In the text to follow, we compare incremental compliances of the Hertzian contact with the ones of the "welded" area of the same elliptic cross-section. In order to compare the two, we have to place the two contact types into similar setting. For this reason, we rephrase results for the Hertzian contact in terms of the extra compliance due to the contact, by assuming that the contacting parts have the configuration of two cylinders

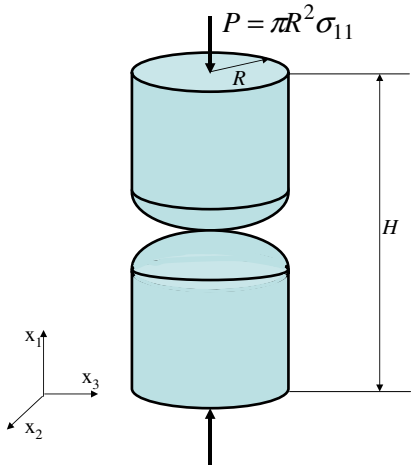

Fig. 4. Elliptic Hertzian contact of two cylinders of radius R and combined length H compressed by stress σ_{11}.

of radius R and combined length H, with contacting asperities; the Hertzian contact is elliptic, with semiaxes a and b (Fig. 4). The cylinders are compressed by stress σ_{11} that is sufficiently small as not to significantly change a (for calculation of the *incremental* compliance). Taking into account that the force transmitted through the contact is $\pi R^2\sigma_{11}$, the representative volume $V=\pi R^2 H$ and strain $\varepsilon_{11}=\delta/H$, the incremental normal compliance of the Hertzian contact takes the form

$$\frac{d\varepsilon_{11}}{d\sigma_{11}}=\Delta S_{1111}=\frac{\pi R^4}{V}\frac{\sqrt{\pi}(1-\nu_0^2)}{E_0}\frac{1}{\sqrt{A}}\frac{2\sqrt{\gamma}}{\pi}\mathcal{K}=\frac{\pi R^4}{V}z_n \tag{2.6}$$

Similarly,

$$\frac{d\varepsilon_{12}}{d\sigma_{12}}=\Delta S_{1212}=\frac{\pi R^4}{V}z^{(a)};\quad \frac{d\varepsilon_{13}}{d\sigma_{13}}=\Delta S_{1313}=\frac{\pi R^4}{V}z^{(b)} \tag{2.7}$$

2.2. Compliances of the elliptic "welded" area

We treat the "welded" area as an *external elliptic crack*, and derive its compliance using Rice's (1975) theorem that relates the crack compliance to stress intensity factors (SIFs), as follows. For a reference volume V containing a crack, the change ΔS_{ijkl} of the overall compliance due to propagation of crack front over additional area ΔA is given by

$$\Delta S_{ijkl}=\frac{1}{V}\frac{1}{4}\int_{\Delta A}c_{qr}\frac{\partial K_q}{\partial\sigma_{ij}}\frac{\partial K_r}{\partial\sigma_{kl}}\,dA \tag{2.8}$$

where K_i (i=1, 2, 3) are modes I, II and III SIFs and coefficients c_{qr} relate the near-tip displacement discontinuity to the SIFs at this point:

$$[u_i]=c_{ij}K_j\sqrt{r/2\pi} \tag{2.9}$$

For the isotropic matrix, there is no coupling between mode I and modes (II, III) and

$$c_{ij}=\frac{8(1-\nu_0^2)}{E_0}\begin{bmatrix}1&0&0\\0&1&0\\0&0&\frac{1}{1-\nu_0}\end{bmatrix} \tag{2.10}$$

Hence, K_I is the only SIF relevant for the *normal* displacement discontinuity $[u_1]$ so that c_{11} is the only relevant coefficient and the integrand in (2.8) reduces to $c_{11}(\partial K_I/\partial\sigma_{11})^2$.

The SIF along the edge of the external elliptic crack, with force P transmitted through the crack, was given by Kassir and Sih (1975):

$$K_I=\frac{P}{2\sqrt{\pi ab}[a^2\sin^2\beta+b^2\cos^2\beta]^{1/4}} \tag{2.11}$$

where angle β characterizes the radial line drawn to the point on the circumscribed circle shown in Fig. 4. For our calculation, however, it is more convenient to use the polar angle ϕ. In its terms, the SIF takes the form (Fabrikant, 1987):

$$K_I=\frac{P}{2\sqrt{\pi ab}}\left(\frac{a^2\sin^2\phi+b^2\cos^2\phi}{a^4\sin^2\phi+b^4\cos^2\phi}\right)^{1/4} \tag{2.12}$$

Rice's (1975) theorem (2.8) requires the SIF to be expressed in terms of stress and not force. Hence, we modify the problem, by replacing half spaces by a circular cylinder of radius R that contains the elliptic cut with semiaxes a, b and assume that $R\gg a,b$ (deep cut). Then $P=\sigma_{11}\pi R^2$ in the formula above and we apply the theorem to propagation of the external elliptic crack from the initial ellipse with semiaxes A,B to the final one, with semiaxes a, b, in such a way that $a,b\ll A,B\ll R$ and the shrinking ellipses remain concentric (constant γ). Calculating integral $\int_{\Delta A}(\partial K_I/\partial\sigma_{11})^2\,dA$ in the polar coordinate system yields:

$$\int_{\Delta A}(\partial K_I/\partial\sigma_{11})^2\,\mathrm{d}A = -\frac{\pi R^4\gamma^2}{4}\int_{-\pi}^{\pi}\frac{\mathrm{d}\phi}{(\sin^2\phi+\gamma^2\cos^2\phi)\sqrt{\sin^2\phi+\gamma^4\cos^2\phi}}\int_{A\gamma(\sin^2\phi+\gamma^2\cos^2\phi)^{-1/2}}^{a\gamma(\sin^2\phi+\gamma^2\cos^2\phi)^{-1/2}}\rho^{-2}\,\mathrm{d}\rho$$
$$= \frac{\pi R^4\gamma}{4a}\int_{-\pi}^{\pi}\frac{\mathrm{d}\phi}{\sqrt{\sin^2\phi+\gamma^2\cos^2\phi}\sqrt{\sin^2\phi+\gamma^4\cos^2\phi}} = \frac{\pi R^4}{a}\mathcal{K} \tag{2.13}$$

where $\rho=\rho(\phi)=\bar{a}\gamma(\sin^2\phi+\gamma^2\cos^2\phi)^{-1/2}$ is the radial distance from the origin of coordinates to a point of a "current" ellipse, with the major semiaxis $\bar{a}$ (contribution from the lower limit of the inner integral vanishes). In the last equality in (2.13) we used the following rule of transformation of the elliptic integrals (see, for example, Korn and Korn, 1968):

$$\mathcal{K}(k)=\frac{2}{1+k'}\mathcal{K}\left(\frac{1-k'}{1+k'}\right) \tag{2.14}$$

where $k'=\sqrt{1-k^2}$ is complementary elliptic modulus. Then substitution of (2.13) and (2.10) into (2.8) yields

$$\Delta S_{1111}=\frac{1}{V}\frac{2\pi R^4}{a}\frac{1-\nu_0^2}{E_0}\mathcal{K}=\frac{1}{V}\frac{2\pi R^4\sqrt{\pi}}{\sqrt{A}}\frac{1-\nu_0^2}{E_0}\sqrt{\gamma}\mathcal{K} \tag{2.15}$$

Remark. The compliance of the external elliptic crack is found in the framework of linear elastic model that does not differentiate between tension and compression. Its applicability to the compressive conditions depends on the magnitude of stress, in relation to the stress that is needed to close the crack and that depends on the initial opening of the crack. We assume that the initial opening is finite, albeit small, and that the applied compressive stress is sufficiently low.

We now examine the tangential compliance of the "welded" area of the same elliptic shape, utilizing results for modes II and III SIFs along the edge of the external elliptic crack generated by shear force. It is sufficient to consider tractions parallel to ellipse's axes (compliance in any other tangential direction is obtained from the tensor relation (2.5)). The SIFs (see Murakami, 1987) written in terms of angle β (Fig. 5) are as follows.

Loading in the direction of semiaxis a produces the following SIFs:

$$\left.\begin{aligned} K_{\mathrm{II}} &= \frac{Q^a b\cos\beta}{2\sqrt{\pi ab}[a^2\sin^2\beta+b^2\cos^2\beta]^{3/4}} \\ K_{\mathrm{III}} &= -\frac{Q^a a\sin\beta}{2\sqrt{\pi ab}[a^2\sin^2\beta+b^2\cos^2\beta]^{3/4}} \end{aligned}\right\} \tag{2.16}$$

where, consistently with the configuration of two cylinders, $Q^a=\sigma_{12}\pi R^2$. Results for loading in the direction of semiaxis b are given by

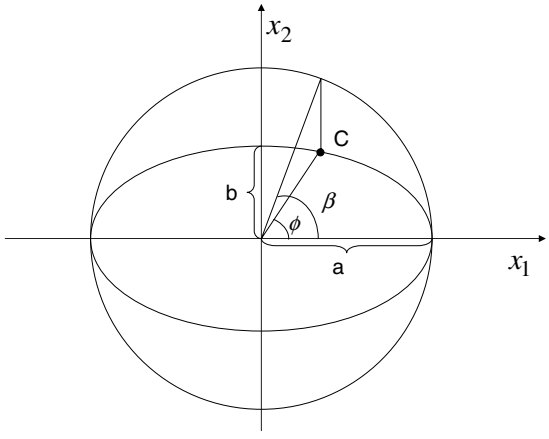

Fig. 5. Angles β and ϕ that are used to identify a current point on the ellipse in Eqs. (2.16), (2.17) and (2.18), (2.19).

$$\left.\begin{aligned} K_{\mathrm{II}} &= \frac{Q^a a \sin\beta}{2\sqrt{\pi ab}\left[a^2\sin^2\beta + b^2\cos^2\beta\right]^{3/4}} \\ K_{\mathrm{III}} &= \frac{Q^b b \cos\beta}{2\sqrt{\pi ab}\left[a^2\sin^2\beta + b^2\cos^2\beta\right]^{3/4}} \end{aligned}\right\} \tag{2.17}$$

with $Q^b = \sigma_{13}\pi R^2$.

For the integration in Rice's (1975) theorem (2.8), it is more convenient to use the polar angle ϕ (similarly to the case of normal loading). Then the SIFs for the loadings parallel to the semiaxes a and b take the form, correspondingly:

$$\left.\begin{aligned} K_{\mathrm{II}} &= \frac{Q^a b\left[a^2\sin^2\phi + b^2\cos^2\phi\right]^{7/4}}{2\sqrt{\pi ab}\left[a^4\sin^2\phi + b^4\cos^2\phi\right]^{5/4}} \\ K_{\mathrm{III}} &= -\frac{Q^a a(a^2-b^2)\sin\phi\cos\phi\left[a^2\sin^2\phi + b^2\cos^2\phi\right]^{3/4}}{2\sqrt{\pi ab}\left[a^4\sin^2\phi + b^4\cos^2\phi\right]^{5/4}} \end{aligned}\right\} \tag{2.18}$$

and

$$\left.\begin{aligned} K_{\mathrm{II}} &= \frac{Q^b a(a^2-b^2)\sin\phi\cos\phi\left[a^2\sin^2\phi + b^2\cos^2\phi\right]^{3/4}}{2\sqrt{\pi ab}\left[a^4\sin^2\phi + b^4\cos^2\phi\right]^{5/4}} \\ K_{\mathrm{III}} &= \frac{Q^b b\left[a^2\sin^2\phi + b^2\cos^2\phi\right]^{7/4}}{2\sqrt{\pi ab}\left[a^4\sin^2\phi + b^4\cos^2\phi\right]^{5/4}} \end{aligned}\right\} \tag{2.19}$$

Calculation of the compliance contribution of the crack yields

$$\begin{aligned} \Delta S_{1212} &= \frac{1}{V}\frac{1}{4}\frac{8(1-\nu_0^2)}{E_0}\int_{\Delta A}\left(\partial K_{\mathrm{II}}/\partial\sigma_{12}\right)^2 + \frac{1}{1-\nu_0}\left(\partial K_{\mathrm{III}}/\partial\sigma_{12}\right)^2 \mathrm{d}A \\ &= \frac{\pi^2 R^4}{V}\frac{1+\nu_0}{\sqrt{\pi}E_0}\frac{1}{\sqrt{A}}\sqrt{\gamma}\left[\left(2-\nu_0+\nu_0\frac{1+\gamma^2}{1-\gamma^2}\right)\mathcal{K} - 2\nu_0\frac{1}{1-\gamma^2}\mathcal{E}\right] \end{aligned} \tag{2.20}$$

and

$$\begin{aligned} \Delta S_{1313} &= \frac{1}{V}\frac{1}{4}\frac{8(1-\nu_0^2)}{E_0}\int_{\Delta A}\left(\partial K_{\mathrm{II}}/\partial\sigma_{13}\right)^2 + \frac{1}{1-\nu_0}\left(\partial K_{\mathrm{III}}/\partial\sigma_{13}\right)^2 \mathrm{d}A \\ &= \frac{\pi^2 R^4}{V}\frac{1+\nu_0}{\sqrt{\pi}E_0}\frac{1}{\sqrt{A}}\sqrt{\gamma}\left[\left(2-\nu_0-\nu_0\frac{1+\gamma^2}{1-\gamma^2}\right)\mathcal{K} + 2\nu_0\frac{1}{1-\gamma^2}\mathcal{E}\right] \end{aligned} \tag{2.21}$$

where transformation rules for elliptic integrals (see, for example, Korn and Korn, 1968) are utilized.

These results coincide, again, with the ones for the shear compliance of the *Hertzian* contact, formula (2.3). Thus, the compliance tensor (2.4) of the Hertzian contact fully applies to the "welded" area of the same geometry. This means that the exact morphology of a contact does not need to be known, as far as its incremental compliance is concerned.

Remark. The fact that the two contact types – the Hertzian and the "welded" ones – have the same compliance becomes clear, if Hill's (1963) auxiliary, or comparison, theorem is recalled. It bounds the compliance of the configuration – in our case, two contacting bodies – by the ones of inscribed and circumscribed geometries. The cusp-like geometry of the Hertzian contact and the elliptical near-tip geometry of the external crack can be bounded by one another as tightly as desired. We note that a somewhat similar conclusion was reached by Mavko and Nur (1978) in a different context of a two dimensional crack of non-elliptical shape.

3. Comparison of the external- and internal crack compliances

It is instructive to compare compliances of the external crack to the ones of the *internal* crack of the same elliptic shape.

For the internal crack, the crack compliance tensor $\boldsymbol{B}$ is defined as tensor that relates the average displacement discontinuity vector across the crack $\boldsymbol{b} \equiv \langle \boldsymbol{u}^+ - \boldsymbol{u}^- \rangle$ to the traction vector $\boldsymbol{\sigma} \cdot \boldsymbol{n}$ induced at the crack site by far-field stress $\boldsymbol{\sigma}$ (Kachanov, 1992):

$$\boldsymbol{b} = \boldsymbol{B} \cdot \boldsymbol{\sigma} \cdot \boldsymbol{n} \tag{3.1}$$

The normal compliance of the internal crack and its tangential compliances in the directions a and b (to within a normalizing multiplier related to the representative volume) are given by the following formulas (that follow from calculations of Budiansky and O'Connell, 1976):

$$B_n = \frac{8(1-\nu_0^2)}{3\sqrt{\pi}E_0}\sqrt{A}\ \underbrace{\frac{\sqrt{\gamma}}{\mathcal{E}}}_{\text{Shape factor}}, \quad B_\tau^{(a)} = \frac{8(1-\nu_0^2)}{3\sqrt{\pi}E_0}\sqrt{A}\ \underbrace{\sqrt{\gamma}Q}_{\text{Shape factor}}, \quad B_\tau^{(b)} = \frac{8(1-\nu_0^2)}{3\sqrt{\pi}E_0}\sqrt{A}\ \underbrace{\sqrt{\gamma}R}_{\text{Shape factor}} \tag{3.2}$$

where

$$Q = \frac{k^2}{(k^2+\nu_0\gamma^2)\mathcal{E} - \nu_0\gamma^2\mathcal{K}}, \quad R = \frac{k^2}{(k^2-\nu_0)\mathcal{E} + \nu_0\gamma^2\mathcal{K}} \tag{3.3}$$

and $k^2 = 1-\gamma^2$; here, $\mathcal{E}$ and $\mathcal{K}$ are the same elliptic integrals that enter (2.2) and (2.3). Note that, in the limits $\gamma \to 1$ and $\gamma \to 0$,

$$\lim_{\gamma\to 1} Q = \lim_{\gamma\to 1} R = \frac{4}{\pi(2-\nu_0)}; \quad \lim_{\gamma\to 0} Q = 1; \quad \lim_{\gamma\to 0} R = \frac{1}{1-\nu_0}$$

Normalized compliances (3.2) are plotted in Fig. 6. They can be compared with the ones for the external crack plotted in Figs. 1–3. An additional comparison of the two cracks, in the context of their tangential anisotropies, is given in Fig. 7.

For both cracks, the tangential anisotropy is relatively mild. The main difference between the two cracks are that the compliances of the external crack are less sensitive to various factors; more specifically,

- Compliances of the external crack are less sensitive to deviations of the elliptic shape from the circular one.
- The tangential anisotropy is less pronounced for the external crack.
- The sensitivity to Poisson's ratio ν_0 is weaker for the external crack.

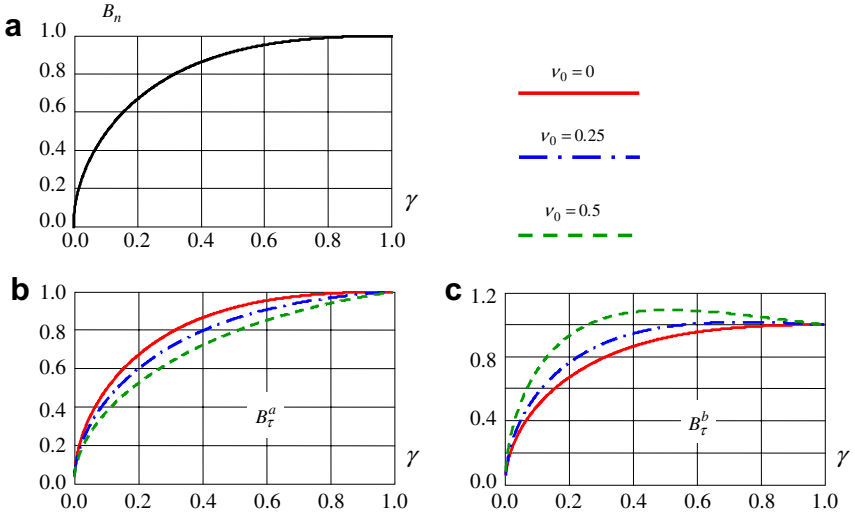

Fig. 6. Normal (a) and shear (b and c, in the directions of major and minor ellipse's axes, respectively) compliances of the *internal* elliptic crack, normalized to their values for a circle.

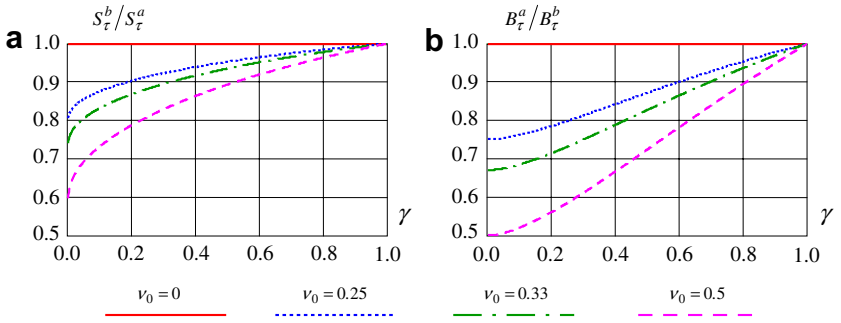

Fig. 7. Comparison of in-plane anisotropies of the tangential compliances of the external (a) and the internal (b) elliptic cracks.

4. Incremental compliances of an interface with multiple elliptic contacts

We consider an interface formed by multiple elliptic contacts and examine its incremental compliances, normal and tangential. The ellipses may have diverse sizes and eccentricities. Their orientation distribution affects the *shear* compliance but is irrelevant for the *normal* compliance. As shown above, the nature of the contacts – whether they are Hertzian or represent "welded" areas – is unimportant for the incremental compliances.

The following assumptions are made:

1. The contacting plates are sufficiently thick, so that bending displacements can be ignored. This implies that all the contacts share the same displacement and can be modeled as parallel springs.
2. The contacts can be considered as non-interacting ones. This is justified by the fact that the overall contact area rarely exceeds 1–2% (see, for example, review of Yovanovich and Marotta, 2003) so that typical spacing between contacts is an order of magnitude larger than sizes of the contact areas. In some cases related to rock mechanics this proportion may be much higher – up to 25% (Pyrak-Nolte et al., 1987). In such extreme cases the results to follow can be viewed as a lower bound for the overall compliance.

We treat the interface as a mathematically thin plane, and represent the contacts-generated displacements as displacement discontinuities $[\boldsymbol{u}] = \boldsymbol{u}^+ - \boldsymbol{u}^-$ across the plane. Then the interface compliance is characterized by second-rank *interface compliance tensor* $\boldsymbol{Z}$ defined by

$$[\boldsymbol{u}] = \boldsymbol{Z} \cdot \boldsymbol{n} \cdot \boldsymbol{\sigma} \tag{4.1}$$

where $\boldsymbol{n}$ is the unit tensor to the interface and $\boldsymbol{\sigma}$ is the remotely applied stress. Its normal component, Z_{nn} characterizes the normal compliance of the interface. If the interface is isotropic with respect to the tangential directions, then,

$$\boldsymbol{Z} = Z_{nn}\boldsymbol{nn} + Z_T(\boldsymbol{I} - \boldsymbol{nn}) \tag{4.2}$$

where Z_T is the shear compliance of the interface. In the general case of anisotropic shear compliance, since tensor $\boldsymbol{Z}$ is symmetric, it has three principal directions of the interface compliance; if the bulk material is isotropic, one of them is $\boldsymbol{n}$ and the other two – the principal directions of the interface compliance $(\boldsymbol{s},\boldsymbol{t})$ – lie in the interface plane:

$$\boldsymbol{Z} = Z_{nn}\boldsymbol{nn} + Z_{ss}\boldsymbol{ss} + Z_{tt}\boldsymbol{tt} \tag{4.3}$$

where (Z_{ss}, Z_{tt}) are the principal shear compliances of the interface.

In the text to follow, we express the normal and shear interface compliances in terms of relevant microstructural parameters.

4.1. Normal compliance

Each of the contacts has the (incremental) compliance given by (2.2) and, since the springs share the same displacement, their stiffnesses are added up, and the incremental Young's modulus E of the interface is given by

$$\frac{E}{E_0} = \frac{1}{1+\sqrt{\pi}(1-\nu_0^2)\xi} \tag{4.4}$$

It is controlled by the dimensionless microstructural parameter

$$\xi = \frac{\bar{A}}{l}\left\langle \frac{\sqrt{A}}{\sqrt{\gamma}\mathcal{K}} \right\rangle^{-1} \tag{4.5}$$

where symbol $\langle \ldots \rangle$ denotes averaging over contacts. It reflects the distribution of contact areas A_m, each taken with its aspect ratio – dependent shape factor $\left(\sqrt{\gamma_m}\mathcal{K}_m\right)^{-1}$. Here, $\bar{A}/l$ is the normalizing factor: l is the overall thickness of the two plates and $\bar{A} = A/N$ is the interface area per one contact, therefore the contribution of the contact zone to the overall compliance depends on the plate thickness l. Expression (4.5) generalizes parameter $\xi = \frac{\bar{A}}{l\langle\sqrt{A}\rangle}$ for the *circular* contacts introduced by Sevostianov and Kachanov (2002). Fig. 1 shows that the parameter for the circular contacts can actually be used, with good accuracy, for the elliptic contacts with aspect ratio $\gamma > 0.4$, i.e. for significantly non-circular shapes.

Remark. The above definition of ξ contains overall thickness l of the two plates as length scale parameter. In rock mechanics, the stiffness is usually defined as the change in sample thickness due to an incremental change in normal stress (see, for example, Jaeger et al., 2007) so that parameter l does not enter the discussion.

Parameter ξ constitutes the proper quantitative characterization of the interface for the normal compliance. It is "proper" in the sense that contributions of individual contacts to ξ correspond to their actual contributions to the overall stiffness.

It is seen that, at the same total contact area (and the same distribution of aspect ratios γ's), *large number of small contacts is stiffer than a small number of large ones*. As far as ellipse eccentricities are concerned, smaller γ's correspond to a stiffer interface (see the plot of the shape factor S_n in Fig. 1). Importantly, these observations apply to both Hertzian and "welded" contacts, as well as their mixtures.

In cases when the distributions over contact areas A's and aspect ratios γ's are statistically independent (thus excluding the situations when larger areas tend to have different shapes than the smaller ones),

$$\xi = \frac{\bar{A}}{l}\left\langle \sqrt{A} \right\rangle^{-1}\left\langle \frac{1}{\sqrt{\gamma}\mathcal{K}} \right\rangle^{-1} \tag{4.6}$$

i.e. parameter ξ contains one average shape factor that decouples from contact areas.

4.2. Shear compliance and its anisotropy: effect of the orientation scatter

The shear compliance depends on the orientation distribution of the ellipses. We first consider the case of random orientations when the shear compliance is isotropic.

We note that, for an individual elliptic contact, its average, over tangential orientations, shear compliance is equal to the average of the two principal values $z^{(a)}$, $z^{(b)}$ given by (2.3), and it differs only by a constant multiplier from the normal compliance of the contact z_n:

$$\langle z_\tau \rangle = \frac{z^{(a)}+z^{(b)}}{2} = \frac{(2-\nu_0)(1+\nu_0)}{\sqrt{\pi}E_0}\frac{1}{\sqrt{A}}\mathcal{K}\sqrt{\gamma} = \frac{2-\nu_0}{2-2\nu_0}z_n \tag{4.7}$$

i.e. it is proportional to shape factor S_n plotted in Fig. 1. As discussed above, if the ellipse aspect ratios $\gamma > 0.4$, z_n can be replaced by its value for a circle, $\sqrt{\pi}(1-\nu_0^2)/(E_0\sqrt{A})$. Moreover, even at small γ, the average $\langle z_\tau \rangle = (z^{(a)}+z^{(b)})/2$ – for example, the average between $z^{(a)}$, $z^{(b)}$ corresponding to γ^2 equal to 0.1 and 10, or to 0.01 and 100 – is close to its value at $\gamma = 1$ (circle). Therefore, formula (4.7) can be used, with good accuracy, even for strongly elongated contact shapes.

In the isotropic case (random ellipse orientations), the average over orientations can be replaced by the average over the in-plane directions of the tangential compliance of a representative ellipse that has average area A and average aspect ratio γ (ergodicity). Then formula (4.7), with A and γ representing the average, over contacts, values, can be applied to the *entire interface*. Thus, the compliance tensor of the interface is given, in the case of random ellipse orientations, by the expression

$$\boldsymbol{Z} = \frac{1+\sqrt{\pi}(1-\nu_0^2)\xi}{E_0}\left[\boldsymbol{nn} + \frac{2-\nu_0}{2-2\nu_0}(\boldsymbol{I}-\boldsymbol{nn})\right] \tag{4.8}$$

where the first and the second terms in the brackets correspond to the normal and shear compliances. Note that a single microstructural parameter ξ controls both the normal and the shear compliances.

We now consider the case of preferential, non-random orientation distribution of elliptic contact areas. This corresponds, for example, to technological processes that have some directionality (such as polishing of a surface by non-circular motions); in geomechanics, this corresponds to anisotropic textures of faults that have undergone sliding. In this case, the shear compliance term in (4.8) has to be replaced by $Z_{ss}\boldsymbol{ss} + Z_{tt}\boldsymbol{tt}$. The principal in-plane compliances Z_{ss}, Z_{tt} and the principal axes $(\boldsymbol{s}, \boldsymbol{t})$ of the tangential compliance reflect the orientation distribution of the ellipses and their distribution over aspect ratios and sizes (the latter two distributions decouple from the orientation distribution in case of their statistical independence). As noted in Section 2, the anisotropy of the tangential compliance of a single elliptic contact is mild, and the same, therefore, applies to the overall shear compliance of the interface, even in the case of ideally parallel ellipses. The anisotropy is further weakened if a preferential orientation of the ellipses is accompanied by noticeable orientation scatter.

We examine these issues for a non-random orientation distribution containing a scatter parameter. The Gaussian distribution would be a natural choice; however, it would lead to results in the numerical form. Therefore, we choose qualitatively similar but somewhat different function that yields explicit results. We assume that the major axes of the ellipses tend to be parallel to x_1 axis (see Fig. 8) and describe the orientation distribution by the following function

$$P_\lambda(\varphi) = \frac{\lambda}{2}\mathrm{e}^{-\lambda|\varphi|} + \frac{1}{\pi}\mathrm{e}^{-\lambda\pi/2} \quad \left(-\frac{\pi}{2} < \varphi < \frac{\pi}{2}\right); \quad \int_{-\pi/2}^{\pi/2} P_\lambda(\varphi)\mathrm{d}\varphi = 1 \tag{4.9}$$

where λ is the scatter parameter; at $\lambda = 0$ and at $\lambda \to \infty$, we have the fully random and the ideally parallel orientations. Fig. 8 shows this distribution for several values of λ.

We represent the vector of force transmitted through the contact as

$$\boldsymbol{F} = F^{(a)}\boldsymbol{e}_a + F^{(a)}\boldsymbol{e}_a \tag{4.10}$$

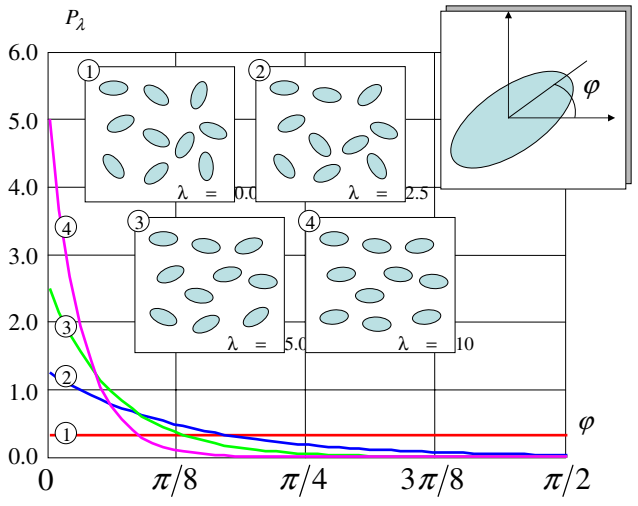

Fig. 8. Orientation distribution function P_λ at several values of scatter parameter λ and the corresponding orientation patterns.

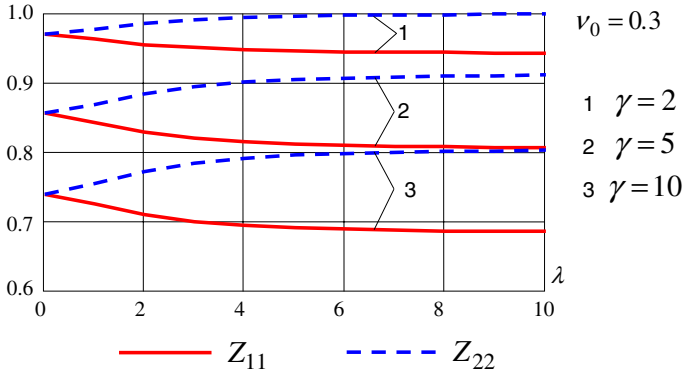

Fig. 9. Tangential compliances Z_{11} and Z_{22} as functions of scatter parameter λ for aspect ratios $\gamma = 2$, 5, 10 and Poisson's ratio $\nu_0 = 0.3$. The difference between the upper and the lower lines characterizes the extent of tangential anisotropy.

where $\boldsymbol{e}_a$, $\boldsymbol{e}_b$ are unit vectors along the ellipse's axes. Taking into account that $F^{(a)} = u^{(a)}/z^{(a)}$, $F^{(b)} = u^{(b)}/z^{(b)}$, that $u^{(a)} = u_1\cos\varphi + u_2\sin\varphi$, $u^{(b)} = -u_1\sin\varphi + u_2\cos\varphi$ and that $\boldsymbol{e}_a = \cos\varphi\boldsymbol{e}_1 + \sin\varphi\boldsymbol{e}_2$, $\boldsymbol{e}_b = -\sin\varphi\boldsymbol{e}_1 + \cos\varphi\boldsymbol{e}_2$, and expressing components F_1,F_2 in terms of u_1,u_2 we have the following expression for the tensor $\boldsymbol{w} \equiv \boldsymbol{z}^{-1}$ defined by $\boldsymbol{F} = \boldsymbol{w}\cdot\boldsymbol{u}$ that can be called *the contact stiffness tensor*:

$$\boldsymbol{w} = \left(\frac{1}{z^{(a)}}\cos^2\varphi + \frac{1}{z^{(b)}}\sin^2\varphi\right)\boldsymbol{e}_1\boldsymbol{e}_1 + \left(\frac{1}{z^{(a)}}\sin^2\varphi + \frac{1}{z^{(b)}}\cos^2\varphi\right)\boldsymbol{e}_2\boldsymbol{e}_2 + \left(\frac{1}{z^{(a)}} - \frac{1}{z^{(b)}}\right)\sin\varphi\cos\varphi(\boldsymbol{e}_1\boldsymbol{e}_2 + \boldsymbol{e}_2\boldsymbol{e}_1) \tag{4.11}$$

Integration $\int_{-\pi/2}^{\pi/2}\boldsymbol{w}(\varphi)P_\lambda(\varphi)\mathrm{d}\varphi$ yields components of the compliance tensor $\boldsymbol{W} = \boldsymbol{Z}^{-1}$ of the interface:

$$\begin{aligned} W_{11} &= \frac{4-\lambda^2\mathrm{e}^{-\lambda\pi/2}}{2(4+\lambda^2)}\frac{1}{z^{(a)}} + \frac{4+2\lambda^2+\lambda^2\mathrm{e}^{-\lambda\pi/2}}{2(4+\lambda^2)}\frac{1}{z^{(b)}} \\ W_{22} &= \frac{4+2\lambda^2+\lambda^2\mathrm{e}^{-\lambda\pi/2}}{2(4+\lambda^2)}\frac{1}{z^{(a)}} + \frac{4-\lambda^2\mathrm{e}^{-\lambda\pi/2}}{2(4+\lambda^2)}\frac{1}{z^{(b)}} \\ W_{12} &= 0 \end{aligned} \tag{4.12}$$

In the limiting cases of fully random and ideally parallel orientations, $2W_{11} = 2W_{22} = (1/Z^{(a)} + 1/Z^{(b)})$ and $W_{11} = 1/Z^{(a)}$, $W_{22} = 1/Z^{(b)}$, respectively.

Since $\boldsymbol{W}$ is symmetric second-rank tensor, the principal values of $\boldsymbol{Z}$ (plotted in Fig. 9) are obtained by inversion of the principal values of $\boldsymbol{W}$: $Z_{11} = W_{11}^{-1}$ and $Z_{22} = W_{22}^{-1}$. It is seen that Z_{11} is generally close to Z_{22}: the tangential anisotropy is mild even for ideally parallel ellipses, and even a moderate orientation scatter makes it weak.

5. Discussion and conclusions

We examined the incremental compliances, normal and tangential, of an interface of two rough surfaces with multiple contacts of the elliptic shape – the shape that takes place for any two locally smooth asperities pressed against one another. The incremental compliances are relevant for the stress levels that are sufficiently low, as not to cause significant changes or to produce new contacts. This is the case, for example, for typical applications involving stress waves, such as ultrasonics. The elliptic contacts may have diverse sizes and aspect ratios and their orientation distribution may be either random or non-random.

We found that effects of the Hertzian contacts and of "welded" areas of the same geometry on the incremental compliances of the interface are identical. This means that the exact morphology of contacts is irrelevant, as far as the incremental compliances are concerned. This statement, obviously, does not apply to nonlinearities under increasing loads (in which case the two contact types behave differently).

Other findings can be summarized as follows.

1. The *normal* compliance of an individual elliptic contact – whether it is Hertzian or represents a welded area – is proportional to the ratio $S_n/\sqrt{A}$ where S_n is the shape factor for the normal mode, that changes from 1 for a circle to zero for a very elongated ellipse. A non-circular contact is stiffer that the circular one of the same area A, although at aspect ratios $\gamma > 0.4$ the difference between them is small.
2. The *shear* compliance of an elliptic contact depends on the in-plane direction, and is controlled by the shape factor for shear, S_τ that is different from S_n. However, this orientation dependence is only moderate and vanishes altogether at Poisson's ratio $\nu_0 = 0$. The *average* over the in-plane directions tangential compliance coincides, to within a multiplier, with the normal compliance and is controlled by the same factor $S_n/\sqrt{A}$.
3. For the *entire interface*, the normal compliance is controlled by the microstructural parameter ξ that is the average of the ratio $\sqrt{A}/S_n$ for individual contacts. It reflects the distribution of contact areas A, each taken with its shape factor. In cases when the distributions over areas and over aspect ratios are statistically independent, ξ decouples into the product of two averages, $\langle\sqrt{A}\rangle\langle 1/S_n\rangle$. For the *circular* shapes, the microstructural characterization simplifies to $\langle\sqrt{A}\rangle$, i.e. *the interface compliance is controlled by the sum of square roots of contact areas (and not by the total contact area!*). This simplified parameter can actually be used, with good accuracy, for the elliptic contacts with aspect ratio $\gamma > 0.4$, i.e. for significantly non-circular shapes.
4. The *shear* compliance of the interface is isotropic in the case of *random* orientation distribution of the ellipses, and it is controlled by the same microstructural parameter ξ as the normal compliance.
5. In the case of *non-random* (preferential) orientations of the ellipses, the shear compliance of the interface is anisotropic. However, the anisotropy is mild, even for ideally parallel ellipses, and is further weakened if orientation scatter is present.

We emphasize that our results hinge on identification of the microstructural parameters that control the incremental compliances (for example, the finding on identical effects produced by the Hertzian contacts and by "welded" areas is rooted in identical microstructural parameters that control them). These parameters are "proper" in the sense that they represent individual contacts in accordance with their actual contributions to the overall stiffness. In this connection, we mention a more general discussion of the proper microstructural parameters given by Kachanov and Sevostianov (2005) in the context of materials with inhomogeneities.

Results for compliances of the external elliptic crack – that appear to be new – are compared with the ones for the *internal* crack of the same elliptic geometry. Both cracks have mild tangential anisotropy; it is somewhat weaker for the external crack. The latter is also less sensitive to factors such as deviations of the elliptic shape from the circular one Poisson's ratio ν_0.

Acknowledgements

The first author (I.S.) acknowledges partial support of NASA (grant to NMSU). The second author (M.K.) acknowledges partial support of NSF (grant to Tufts University).

References

Baltazar, A., Rokhlin, S., Pecorari, C., 2002. On the relationship between ultrasonic and micromechanical properties of contacting rough surfaces. Journal of the Mechanics and Physics of Solids 50, 1397–1416.

Budiansky, O'Connell, 1976. Elastic moduli of a cracked solid. International Journal of Solids and Structures 12, 81–97.

Fabrikant, V., 1987. The stress intensity factor for an external elliptical crack. International Journal of Solids and Structures 23 (4), 465–467.

Hill, R., 1963. Elastic properties of reinforced solids: some theoretical principles. Journal of the Mechanics and Physics of Solids 11, 357–372.

Jaeger, J.C., Cook, N.G.W., Zimmerman, R.W., 2007. Fundamentals of Rock Mechanics. Blackwell Publ.

Johnson, K.L., 1985. Contact Mechanics. Cambridge University Press.

Kachanov, M., 1992. Effective elastic properties of cracked solids: critical review of some basic concepts. Applied Mechanics Reviews 45 (8), 305–336.

Kachanov, M., Sevostianov, I., 2005. On quantitative characterization of microstructures and effective properties. International Journal of Solids and Structures 42, 309–336.

Kassir, M.K., Sih, G., 1975. Three-dimensional Crack Problems. Noordhoff, Leyden (Chapter 4).
Korn, G.A., Korn, T.M., 1968. Mathematical Handbook for Scientists and Engineers. McGraw Hill, New York (Chapter 21).
Mavko, G.M., Nur, A., 1978. The effect of nonelliptical cracks on the compressibility of rocks. Journal of Geophysical Research 83 (B-9), 4459–4468.
Mindlin, R.D., 1949. Compliance of elastic bodies in contact. Journal of Applied Mechanics 16, 259–268.
Murakami, Y. (Ed.), 1987. Stress Intensity Factors Handbook, vol. 2. Pergamon.
Nagy, P.B., 1992. Ultrasonic classification of imperfect interfaces. Journal of Nondestructive Evaluation 11 (3/4), 127–139.
Pyrak-Nolte, L.J., Myer, L.R., Cook, N.G.W., Witherspoon, P.A., 1987. Hydraulic and mechanical properties of natural fractures in low permeability rock. In: Herget, G., Vongpaisal, S. (Eds.), Proc. of 6th Int. Cong. Rock Mech.. Balkema, Rotterdam, pp. 225–231.
Rice, J.R., 1975. Continuum mechanics and thermodynamics of plasticity in relation to microscale deformation mechanisms. In: Argon, A. (Ed.), Constitutive Equations in Plasticity. MIT Press, pp. 23–75.
Sevostianov, I., Kachanov, M., 2002. Explicit cross-property correlations for anisotropic two-phase composite materials. Journal of the Mechanics and Physics of Solids 50, 253–282.
Sevostianov, I., Kachanov, M., 2008. Contact of rough surfaces: a simple model for elasticity, conductivity and cross-property connections. Journal of the Mechanics and Physics of Solids. doi:10.1016/j.jmps.2007.09.004.
Walsh, J., Zhu, W., 2004. Sliding of a rough surface under oblique loading. Journal of Geophysical Research 109, B05208–B05217.
Yovanovich, M.M., Marotta, E.E., 2003. Thermal spreading and contact resistances. In: Bejan, A., Krauf, A.D. (Eds.), Heat Transfer Handbook. John Wiley, pp. 261–393.
Zimmerman, R.W., Chen, D.W., Cook, N.G.W., 1992. The effect of contact area on the permeability of fractures. Journal of Hydrology 139, 79–96.